Hindawi Publishing Corporation
Journal of Chemistry
Volume 2015, Article ID 532198, 9 pages
http://dx.doi.org/10.1155/2015/532198

Research Article

Magnetic Properties and AC Losses in AFe_2O_4 (A = Mn, Co, Ni, Zn) Nanoparticles Synthesized from Nonaqueous Solution

Oleksandr Yelenich,[1] Sergii Solopan,[1] Taras Kolodiazhnyi,[2] Yuliya Tykhonenko,[3] Alexandr Tovstolytkin,[3] and Anatolii Belous[1]

[1]*Institute of General and Inorganic Chemistry, 32/34 Palladina Boulevard, Kyiv 03142, Ukraine*
[2]*National Institute for Materials Science, 1-1 Namiki, Tsukuba, Ibaraki 305-0044, Japan*
[3]*Institute of Magnetism, 36-b Vernadsky Avenue, Kyiv 03142, Ukraine*

Correspondence should be addressed to Sergii Solopan; solopan@ukr.net

Received 9 December 2014; Accepted 17 February 2015

Academic Editor: Fa-Nian Shi

Nanosized particles of AFe_2O_4 (A = Mn, Co, Ni, or Zn) spinel ferrites were synthesized by coprecipitation from nonaqueous solutions using nitrate salts as starting reagents. The particles were characterized by X-ray diffraction, transmission electron microscopy, and magnetic measurements. Quasistatic magnetic measurements show superparamagnetic behavior with blocking temperature below room temperature for cobalt, nickel, and zinc spinel ferrite nanoparticles. Characteristic magnetic parameters of the particles including average magnetic moment of an individual nanoparticle and blocking temperature have been determined. The specific loss power which is released on the exposure of an ensemble of synthesized particles to a magnetic field is calculated and measured experimentally. It is shown that among all nanoferrites under study, the $ZnFe_2O_4$ nanoparticles demonstrate the highest heating efficiency in AC magnetic fields. The key parameters responsible for the heating efficiency in AC magnetic field have been determined. The directions to enhance the SLP value have been outlined.

1. Introduction

Nanosized particles of AFe_2O_4 (A = Mn, Co, Ni, Zn) spinel ferrites are the subject of considerable scientific and practical interest. They can be used in the manufacture of magnetic recording devices, catalysts, sensors, and microwave elements [1–3]. Recently, the nanoparticles (NPs) with spinel structure have been intensely investigated for their further use in biomedical applications. To date, it has been established that the NPs of spinel ferrites may play a leading role in diagnosis of diseases, as contrast agents in magnetic resonance imaging [4]. At the same time, the directions related to the use of the NPs for drug delivery [5], as well as hyperthermia in the treatment of cancer [6, 7], have not been completely investigated and such works become more and more topical.

For the latter two directions, the NPs have to meet a number of special requirements, in particular, to be single-domain ones, be robust against agglomeration, and have controllable sizes ranging from a few nanometers up to tens of nanometers, so that their optimal size can be easily adjusted to match specific biological entity of interest. For the use as hyperthermia agents, the NPs have to satisfy additional requirements: the ensemble of particles has to demonstrate high values of specific loss power (SLP) released upon exposure to AC magnetic field.

It is known that when subjected to AC magnetic field, magnetic NPs can dissipate the energy to their environment by Brownian (particle rotation) and Néel (moment reorientation) relaxation mechanisms [8, 9]. However, the nature of AC losses in the NPs of AFe_2O_4 (A = Mn, Co, Ni, Zn) compounds have not been completely understood. In addition, the physical and chemical parameters that may provide the SLP enhancement have not been determined yet.

Therefore, the aim of this work was to synthesize weakly agglomerated NPs of AFe_2O_4 (A = Mn, Co, Ni, Zn) spinel ferrites, study their magnetic properties, look into the nature

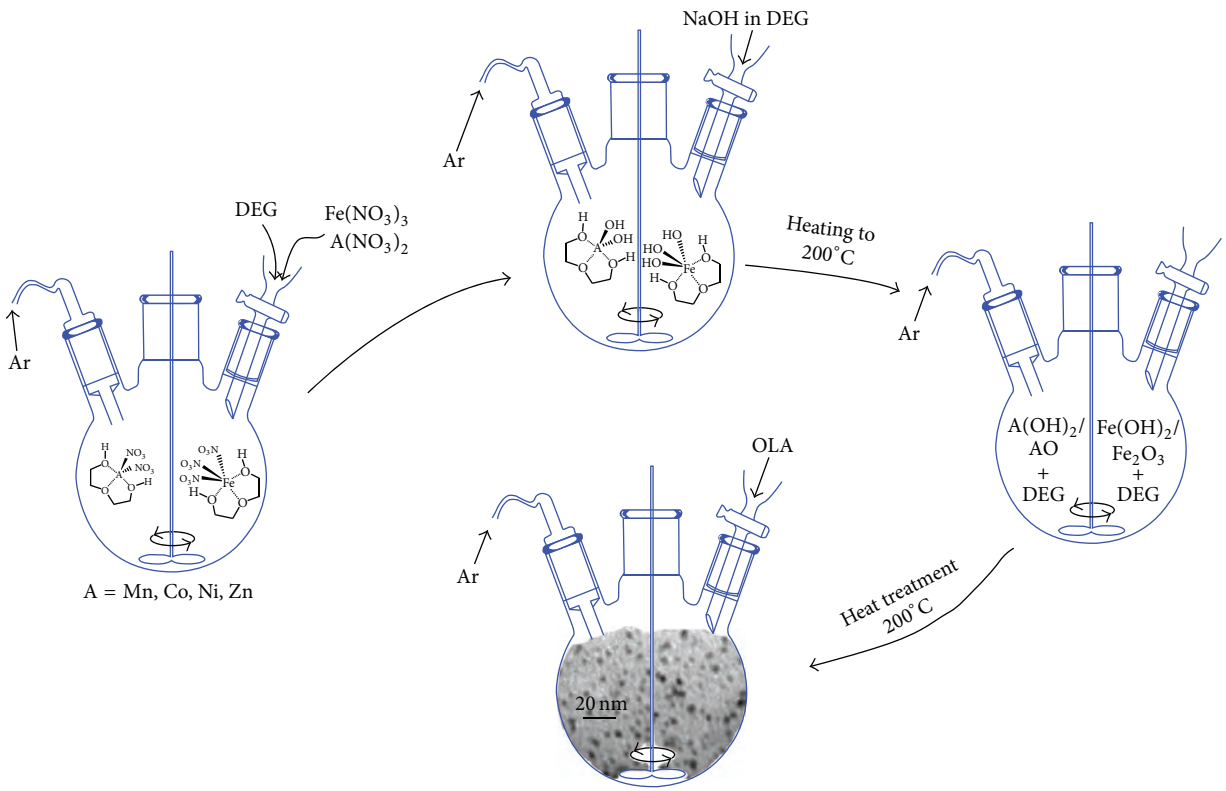

Figur e 1: Synthesis scheme from diethylene glycol solutions for NPs of AFe_2O_4 (A = Mn, Co, Ni, Zn) spinel ferrites.

of AC losses in the ensemble of such NPs, and identify the ways to increase their heating efficiency.

2. Experimental Section

For the synthesis of AFe_2O_4 NPs (A = Mn, Co, Ni, Zn), diethylene glycol was used as the reaction medium, which made it possible to synthesize weakly agglomerated particles with a size of a few nanometers. The synthesis was carried out according to the scheme shown in Figure 1. Starting reagents used for the reactions were nitrate salts. NaOH was used as precipitant of metal oxides. The NPs precipitated in solution were stabilized with oleic acid. Further details of the NPs preparation route were described in [10, 11].

A Specord-M3l infrared spectroscope was used to determine the existence of oleic acid and diethylene glycol on the surface of the as-prepared NPs; the samples were prepared as KBr pellets. Thermal analysis (DTA and DSC) was performed on SDT Q600 instrument. The heating was carried out on Pt plates using α-Al_2O_3 as an inert reference material. The samples were heated up to 1000°C with a heating rate of $5^\circ C\,min^{-1}$.

Obtained powders were investigated by X-ray diffraction analysis (XRD) on a DRON-4 diffractometer (CuKα radiation). Lattice parameters, intensity redistributions, and angles of X-ray peaks for synthesized compounds were refined using the FullProf_Suite software package. NaCl powder was used as an internal standard, while the total deviation from zero point did not exceed 0.01° for all of X-ray diffraction patterns. The crystallite size was estimated from XRD line broadening using the Scherrer equation, $DXRD = K\lambda/B\cos\theta$, with the wave length λ, the peak width of the diffraction peak profile at half maximum height resulting from small crystallite size in radians B, the Bragg angle θ, and the shape factor $K \approx 0.89$ [12]. Calculation of peak width of the X-ray diffraction peak profile at half maximum height was performed using reflections of CuKα1 radiation. For the separation of the diffraction peaks from CuKα1 and CuKα2 radiations the calculations were carried out using the Peak_Fit software with the assumption that the intensity ratio of CuKα1 and CuKα2 is 2 : 1.

The size and morphology of powder particles were analyzed by means of JEOL JEM-1230 transmission electron microscope (TEM) equipped with an energy dispersive spectrometer (EDX) (electron probe diameter: 200 nm). Size distribution was obtained from the analysis of TEM images with the use of Image Tool 3 and OriginPro 8.5 SR1 software packages. When calculating particles size distribution, TEM images were analyzed according to the procedure described by Peddis et al. [13].

Magnetic measurements were performed in the (2 ÷ 300) K temperature range using commercial Quantum Design Magnetic Property Measurements System equipped with superconducting quantum interference device (SQUID). Magnetic moment was measured upon sample heating for both zero-field-cooling (ZFC) and field-cooling (FC) modes. Isothermal magnetic hysteresis loops were measured at 10 and 300 K in the magnetic field of −30 to +30 kOe.

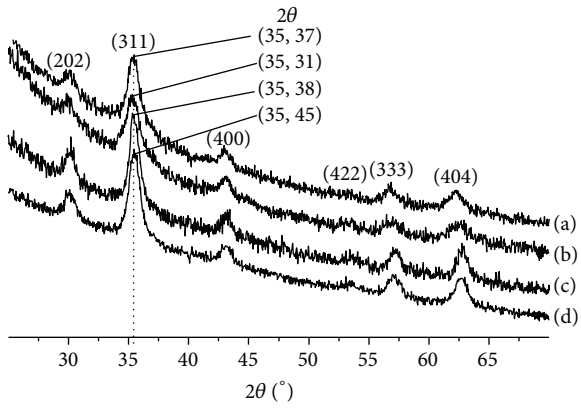

Figure 2: X-ray diffraction patterns for the ferrite powders prepared from diethylene glycol solution at ~200°C: (a) $MnFe_2O_4$; (b) $CoFe_2O_4$; (c) $NiFe_2O_4$; (d) $ZnFe_2O_4$.

The measurement modes employed in this work made it possible to determine coercivity with an inaccuracy of about ±5 Oe.

For the calorimetric determination of SLP, the ferrofluids based on synthesized NPs were prepared using 0.1% aqueous agarose solutions [14] and placed into a coil (5 turns, 30 mm diameter) that provided the AC magnetic field with frequency 300 kHz and amplitudes up to 7.7 kA/m. All calorimetric measurements were performed according to the procedure described by Veverka et al. [15]. SLP values were calculated using formula

$$\mathrm{SLP} = \frac{C_{\mathrm{Fluid}} \cdot V_s}{m_{\mathrm{powder}}} \cdot \frac{\mathrm{d}T}{\mathrm{d}\tau}, \quad (1)$$

where $\mathrm{d}T/\mathrm{d}\tau$ is the initial slope of the graph of the change in temperature versus time, C_{Fluid} and V_s are the volumetric specific heat and volume of the solution, respectively, and m_{powder} is the mass of magnetic material in the fluid.

3. Results and Discussion

The X-ray diffraction patterns for the synthesized NPs are shown in Figure 2. The observed patterns are characteristic of the compounds with a cubic spinel structure (space group *Fd3m*). The refined lattice parameters are listed in Table 1. EDX analysis shows that the A/Fe ratio is very close to 0.5 that corresponds to the formula AFe_2O_4 (A = Mn, Co, Ni, Zn). The crystallite sizes listed in Table 1 were calculated using the broadening of the *hkl* = 311 diffraction peak.

The results of IR spectroscopy of the as-prepared ferrite powders obtained after washing and drying are characterized by the presence of absorption bands of Me–O, $-COO^-$, and C–H chemical bonds indicating the presence of remnants of oleic acid (see [14]). Conducted DTA and DSC studies of the synthesized NPs also confirmed the presence of organic substances, the amount of which was about ~30% of the weight of the synthesized powder (see [11]).

TEM micrographs of the AFe_2O_4 powders (Figure 3) demonstrate that the particles are weakly agglomerated; the distribution of particle sizes seems to be quite narrow and most of the NPs have sizes 3–6 nm.

Table 1: Crystallographic parameters of the AFe_2O_4 (A = Mn, Co, Ni, Zn) NPs.

Parameter	Composition			
	$MnFe_2O_4$	$CoFe_2O_4$	$NiFe_2O_4$	$ZnFe_2O_4$
Parameter *a*, Å	8.384	8.381	8.347	8.433
$a = b = c$				
R_f*	5.2	7.1	3.47	3.2
R_{Bragg}*	4.7	5.3	2.92	2.1
D_{XRD}	7.0	3.5	6.6	6.3
D_{TEM}	6.0 ± 1.7	3.0 ± 0.4	4.9 ± 0.8	4.3 ± 0.9

*Reliability factors.

Figure 4 shows the magnetization M versus magnetic field H dependences for the NPs of zinc, manganese, cobalt, and nickel spinel ferrites. The magnetization curves were obtained at 10 K. The shapes of the $M(H)$ curves are characteristic of magnetically ordered materials: the magnetization rapidly grows at low fields (0–3 kOe), then the growth becomes weaker, and, finally, the magnetization tends to saturate at high fields. The saturation magnetization, M_s, is greatest for the NPs of zinc and manganese ferrites ($M_s^{ZnFe_2O_4, MnFe_2O_4} \approx 70$ emu/g). This is almost two times higher than that of cobalt ferrite ($M_s^{CoFe_2O_4} \approx 36$ emu/g) and a factor of 4.7 higher than that found for nickel ferrite samples ($M_s^{NiFe_2O_4} \approx 15$ emu/g). Except for zinc ferrite NPs, the obtained values of M_s are 1.5–2 times smaller than those reported for the bulk counterparts ($M_s^{MnFe_2O_4\,bulk} \approx 112$ emu/g, $M_s^{CoFe_2O_4\,bulk} \approx 94$ emu/g, $M_s^{NiFe_2O_4\,bulk} \approx 56$ emu/g) [16]. This is likely to result from a noticeable contribution from the subsurface layers of NPs, which, as a rule, are partly or completely magnetically disordered [17].

Among all ferrites, zinc ferrite occupies a special place because it exhibits unusual behavior at nanoscale level. Bulk $ZnFe_2O_4$ has a normal spinel structure, in which all Zn^{2+} ions occupy tetrahedral positions (A-sites) and all Fe^{3+} ions occupy octahedral positions (B-sites). At room temperature, zinc ferrite is paramagnetic, and the transition to a magnetically ordered state occurs only at temperatures of about 10 K [16]. The magnetic properties change significantly when the particle size decreases to a few tens of nanometers: at this scale, a cation inversion occurs; that is, a part of zinc ions occupy the B-sites and part of iron ions occupy the A-sites [17, 18]. Thus, there is a transformation of structure from normal to mixed spinel, which leads to disequilibrium in the system with competing magnetic interactions and, as a rule, to the appearance of resultant spontaneous magnetization. The degree of cation inversion depends on the particle size [17–19]. As a result of such transformations, the magnetization of $ZnFe_2O_4$ NPs can reach sufficiently high values, and this phenomenon seems to be observed in our case (see Figure 4).

For all the NPs under consideration, the M versus H curves are hysteretic at 10 K. The coercivity H_c is maximal in the NPs of cobalt ferrite ($H_c^{CoFe_2O_4} \approx 9$ kOe). It is almost two orders of magnitude larger than the coercivity

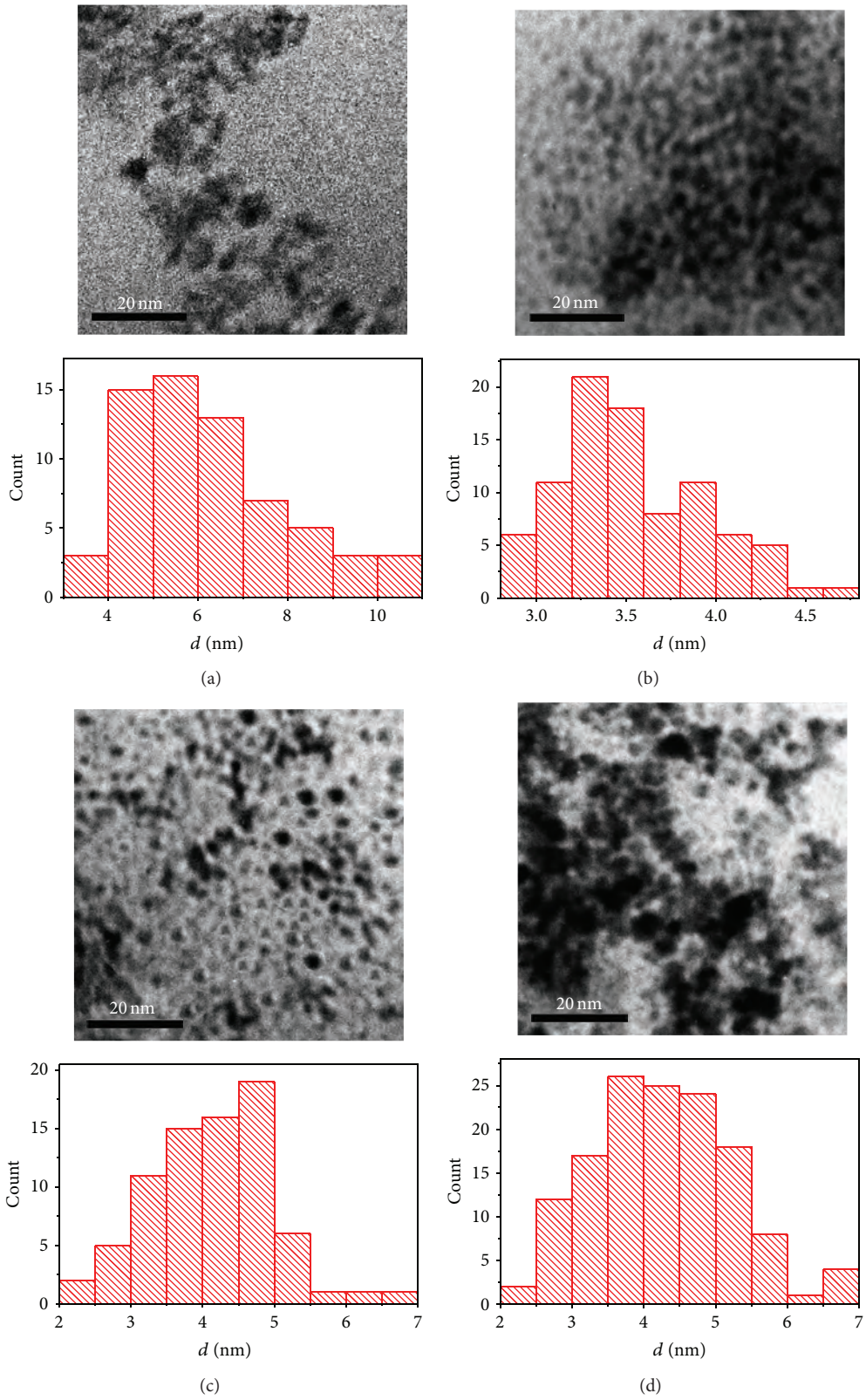

Figur e 3: TEM images of the NPs obtained from a diethylene glycol solution: (a) $MnFe_2O_4$; (b) $CoFe_2O_4$; (c) $NiFe_2O_4$; (d) $ZnFe_2O_4$.

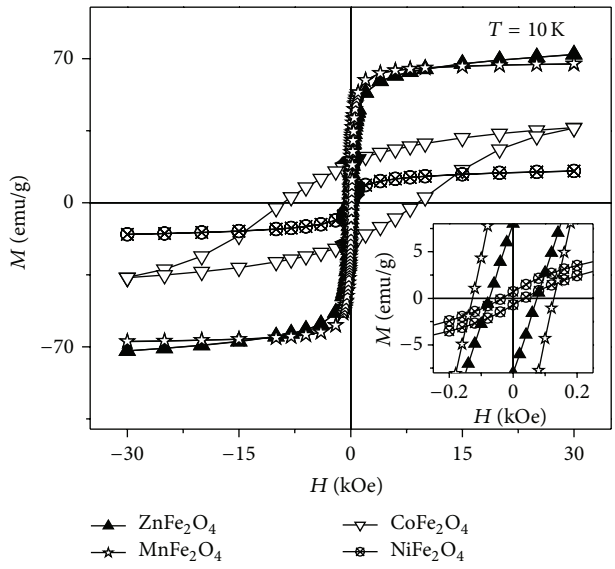

Figur e 4: The magnetization M versus magnetic field H dependences for the NPs of zinc, manganese, cobalt, and nickel spinel ferrites. The magnetization curves were obtained at 10 K. Inset shows the same dependences in the region of low fields.

of the NPs of zinc and manganese ferrites ($H_c^{ZnFe_2O_4} \approx 0.08$ kOe, $H_c^{MnFe_2O_4} \approx 0.13$ kOe). The smallest value of H_c is characteristic of the nickel ferrite NPs ($H_c^{NiFe_2O_4} \approx 0.03$ kOe). It is noteworthy that the coercivity of ferrite NPs is very sensitive to a synthesis method, heat treatment, particle size, and so forth, but, for the same synthesis technique, the coercivity is greatest in cobalt ferrite NPs and few orders smaller in the NPs of nickel ferrite [20, 21]. The results obtained in this paper agree with such tendencies.

Temperature dependences of magnetization (Figure 5) were obtained in two different measurement modes: zero-field-cooling (ZFC) and field-cooling (FC). In the ZFC mode, a sample was cooled in zero magnetic fields down to 2 K. At this temperature, an external magnetic field $H_{measur} = 20$ Oe was applied to the sample and M_{ZFC} was measured as a function of T in the process of sample heating. The FC mode differs in that the sample was cooled in magnetic field $H_{cooling} = H_{measur}$. For the NPs under study, the $M_{FC}(T)$ and $M_{ZFC}(T)$ curves coincide with each other in the vicinity of room temperature but start diverging as temperature is lowered. Each $M_{ZFC}(T)$ curve displays a maximum at a certain temperature T_b ($T_b^{ZnFe_2O_4} \approx 55$ K, $T_b^{MnFe_2O_4} \approx 195$ K, $T_b^{CoFe_2O_4} \approx 140$ K, $T_b^{NiFe_2O_4} \approx 15$ K), which is called a blocking temperature. At the same time, over the whole temperature range studied, M_{FC} increases with the decrease in temperature (for all but zinc ferrite NPs) or displays only a slight decrease below T_b (for zinc ferrite NPs). In the vicinity of room temperature, the curvature of $M_{ZFC}(T)$ and $M_{FC}(T)$ dependences is positive ($d^2M/dT^2 > 0$) for all NPs under study, except for those of manganese ferrite. While the positive curvature of the temperature dependences of magnetization is a prerequisite of superparamagnetic behavior [16, 22], the question whether or not the NPs are superparamagnetic is addressed further on.

Figure 6 shows temperature dependences of reciprocal susceptibility $\chi^{-1}(T)$ for those samples, for which $M_{ZFC}(T)$ and $M_{FC}(T)$ dependences display positive curvature, that is, for the $ZnFe_2O_4$, $CoFe_2O_4$, and $NiFe_2O_4$ NPs. Here, χ^{-1} was determined as H_{measur}/M_{FC}, where H_{measur} is 20 Oe. For superparamagnets, the $\chi^{-1}(T)$ dependences, measured in weak magnetic fields, are linear [22]. In our case, however, linear regions can be singled out only in the vicinity of room temperature. For the NPs of all three spinel ferrites, the $\chi^{-1}(T)$ dependences deviate from linear ones below 220–250 K. T his means that in the temperature region from ~250 K down to T_b, the NPs' behavior is characterized by a complex magnetic ordering.

Figure 7 shows the $M(H)$ dependences obtained at 300 K. Of all the samples under investigation, the NPs of manganese ferrite display the greatest magnetization ($M_{30\,kOe}^{MnFe_2O_4} \approx 42$ emu/g). For these NPs, magnetization is also characterized by a pronounced tendency to saturation in high magnetic fields. For the rest of the samples, the magnetization is smaller ($M_{30\,kOe}^{ZnFe_2O_4,\ CoFe_2O_4} \approx 30$ emu/g, $M_{30\,kOe}^{NiFe_2O_4} \approx 8$ emu/g) and tendency to saturation is far less pronounced. For the $ZnFe_2O_4$ and $CoFe_2O_4$ NPs, the $M(H)$ curves are very close to each other. Coercivity of all the samples is a few Oe, which is within the measurement inaccuracy of the magnetometer.

The results obtained (almost linear $\chi^{-1}(T)$ dependence near 300 K, negligible coercivity, and weakly pronounced tendency of magnetization towards saturation) may testify to the superparamagnetic behavior of the $ZnFe_2O_4$, $CoFe_2O_4$, and $NiFe_2O_4$ NPs at 300 K (the behavior of $MnFe_2O_4$ NPs does not seem to follow these requirements; see Figures 5 and 7). To further confirm these findings, the experimental data were compared with the magnetization curves of an ideal superparamagnet.

The equilibrium magnetization M of an ensemble of superparamagnetic particles placed in magnetic field H at temperature T reads [23]

$$M = n\mu L\left(\frac{\mu H}{kT}\right) \equiv n\mu\left[\coth\left(\frac{\mu H}{kT}\right) - \frac{kT}{\mu H}\right], \qquad (2)$$

where L is the Langevin function [22, 23], n is the concentration of particles, μ is the magnetic moment of a separate particle, and k is the Boltzmann constant.

The results of the fitting of the experimental data with function (2) are shown in Figure 8. The fitting procedure was carried out with the use of a fitting tool of OriginPro 8.5 SR1. The use of such procedure makes it possible to calculate the concentration n and average magnetic moment μ of the particles. With knowing n, one can estimate the upper limit of the particle diameter as $d = n^{-1/3}$ (Table 2).

For the NPs of zinc and nickel spinel ferrites, the value of d calculated from the data of magnetic measurements agrees with the results of electron-microscopic and XRD investigations (see Figure 3). Such correspondence additionally confirms that these particles are characterized by a quite narrow distribution in particle size.

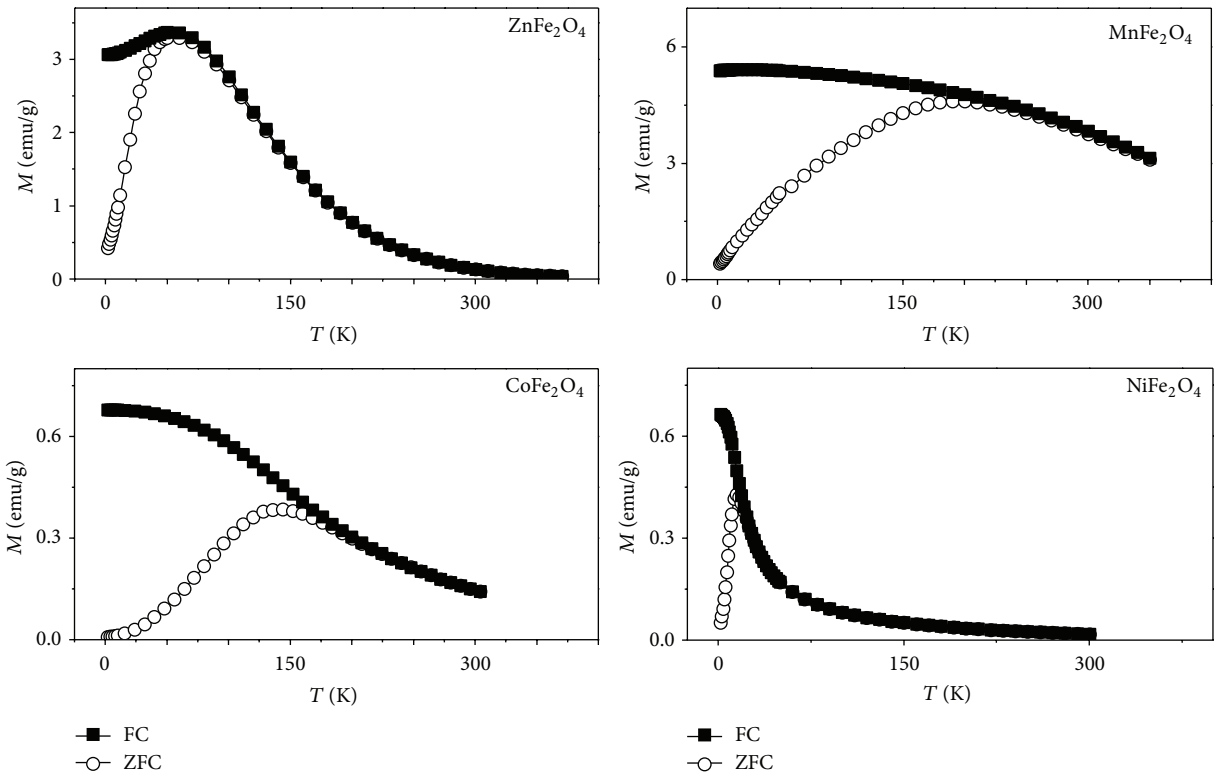

Figur e 5: Temperature dependences of magnetization M (ZFC- and FC-measurements) for the NPs of zinc, manganese, cobalt, and nickel spinel ferrites. Measurements were carried out in magnetic field H_{measur} = 20 Oe.

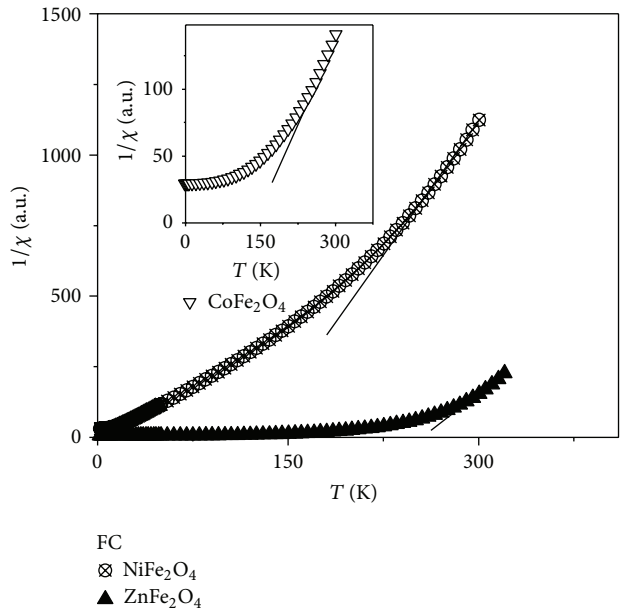

Figur e 6: Temperature dependences of reciprocal susceptibility $\chi^{-1}(T)$ for the NPs of zinc, cobalt, and nickel spinel ferrites.

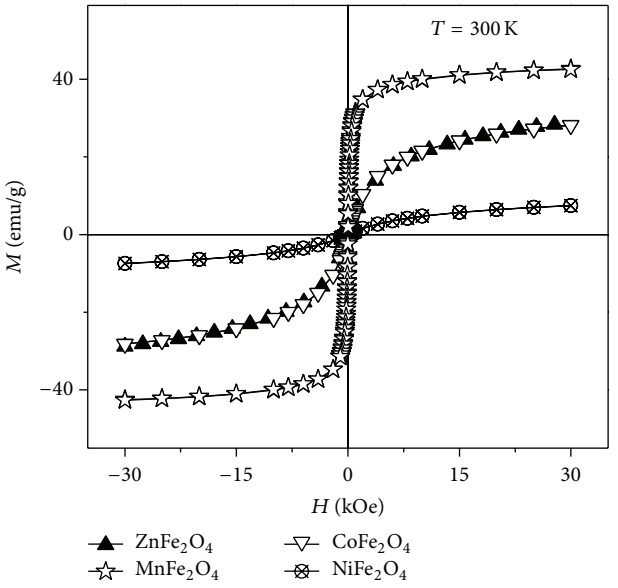

Figur e 7: The magnetization M versus magnetic field H dependences for the NPs of zinc, manganese, cobalt, and nickel spinel ferrites. The magnetization curves were obtained at 300 K.

For the NPs of cobalt spinel ferrite, there is no satisfactory agreement between the fitted and experimental $M(H)$ dependences (Figure 8). The reason for such divergence can lie in a partial agglomeration of the particles or wider distribution in particle size. It is also noteworthy that the $CoFe_2O_4$ NPs are highly anisotropic with high values of coercivity and blocking

Table 2: The average magnetic moment μ and upper limit of particle diameter d calculated from the fitted $M(H)$ curves (μ_B is the Bohr magneton).

	$CoFe_2O_4$	$NiFe_2O_4$	$ZnFe_2O_4$
μ (μ_B)	2555	1010	2032
d (nm)	4.9	5.7	5.0

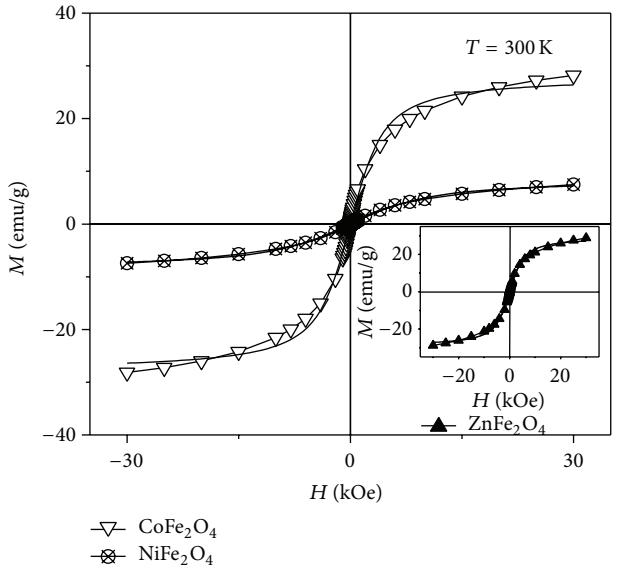

Figure 8: Experimental $M(H)$ dependences obtained at $T = 300$ K (symbols) and results of their fitting by Langevin function (solid lines).

temperature. These can introduce additional complications in their behavior.

The AC losses for the $NiFe_2O_4$, $CoFe_2O_4$, and $ZnFe_2O_4$ NPs placed in an external magnetic field were calculated with the use of the linear response theory using the Neel relaxation time [24]. This model is based on the assumption that the magnetic system responds linearly to the magnetic field and is suitable for calculation of AC losses in superparamagnetic NPs at low magnetic field [25]. According to this model, the specific loss power can be expressed as

$$P = \mu_0 \chi H_0^2 \frac{2\pi^2 f^2 \tau}{1 + (2\pi f \tau)^2}, \quad (3)$$

where μ_0 is the permeability of free space ($\mu_0 = 4\pi \times 10^{-7}$ N/m), χ is the magnetic susceptibility of the ensemble of NPs, H_0 is the amplitude of magnetic field, and f is the frequency of AC magnetic field.

The relaxation time τ can be expressed as

$$\tau = \frac{\sqrt{\pi}}{2} \tau_0 \frac{\exp G}{\sqrt{G}}, \quad (4)$$

where $G = 25T_b/T$, $\tau_0 = 10^{-9}$ s [24].

There are strong medical restrictions imposed on the parameters of AC magnetic fields which are likely to be used in magnetic hyperthermia [15, 24]. This, in particular, concerns the upper limit of the product $H_0 f$ ($H_0 f$ has to be less than 5×10^9 A·m^{-1}·s^{-1}) and the acceptable range of frequencies (the frequency f has to be above 50 kHz to avoid neuromuscular electrostimulation and below 10 MHz to achieve a satisfactory depth of the field penetration into the electrically conducting tissue) [14, 15, 24, 25]. Typical parameters of AC magnetic fields are $f \sim (100 \div 500)$ kHz and $H_0 \leq 400$ Oe [15, 24]. Below, the calculations and measurements of SLP are carried out for the $NiFe_2O_4$, $CoFe_2O_4$, and $ZnFe_2O_4$ NPs placed in AC magnetic field with $f = 300$ kHz and $H_0 = 7.7$ kA/m (98 Oe). With the use of formulae (3)-(4), the SLP values can be recalculated for other parameters of AC magnetic fields.

The SLP values calculated according to formula (3) are

$$P^{NiFe_2O_4} = 1.36 \text{ W/g}, \quad P^{CoFe_2O_4} = 9.7 \text{ W/g}, \quad P^{ZnFe_2O_4} = 32 \text{ W/g}. \quad (5)$$

Magnetic susceptibility, χ, was found from M versus H dependences measured at 300 K (see Figure 7). The values of blocking temperatures were determined from the M versus T dependences (see Figure 5).

The experimental values of SLP, measured for the $NiFe_2O_4$, $CoFe_2O_4$, and $ZnFe_2O_4$ NPs placed in AC magnetic field with the same parameters, are

$$P_{exp}^{NiFe_2O_4} = 1.8 \text{ W/g}, \quad P_{exp}^{CoFe_2O_4} = 8 \text{ W/g}, \quad P_{exp}^{ZnFe_2O_4} = 89 \text{ W/g}. \quad (6)$$

Quite good agreement between the experimental data and calculated ones, observed for the $NiFe_2O_4$ and $CoFe_2O_4$ NPs, along with similar results obtained by other researchers [8, 24], testify to the adequacy of the model used for the SLP calculation. At the same time, the noticeable divergence for the $ZnFe_2O_4$ NPs may imply that the model underestimates the SLP for the NPs with sufficiently high SLP values.

Based on the obtained results, let us analyze which NP parameters are of crucial importance for the SLP value. It follows from formula (3) that SLP is directly proportional to magnetic susceptibility χ, but its dependence on relaxation time τ (which, in turn, is governed by blocking temperature T_b) is nonmonotonous. To find out in which direction the NP parameters should be changed to achieve maximal heating efficiency, we calculated SLP as a function of T_b. The calculations were carried out under the assumption that all magnetic parameters correspond to the parameters of $NiFe_2O_4$ NPs (see Figure 8 and Table 2) and T_b is varied. The results are shown in Figure 9. It follows from the figure that there exists an optimal value of blocking temperature ($T_b \approx 90$ K), realization of which will result in an increase in the SLP up to ~300 W/g under the given magnetic field parameters ($f = 300$ kHz and $H_0 = 7.7$ kA/m).

Thus, the task comes either to finding specific conditions of the synthesis and heat treatment of spinel ferrite NPs or to synthesis of core-shell NPs which (1) have blocking temperature near 90 K, (2) display superparamagnetic behavior

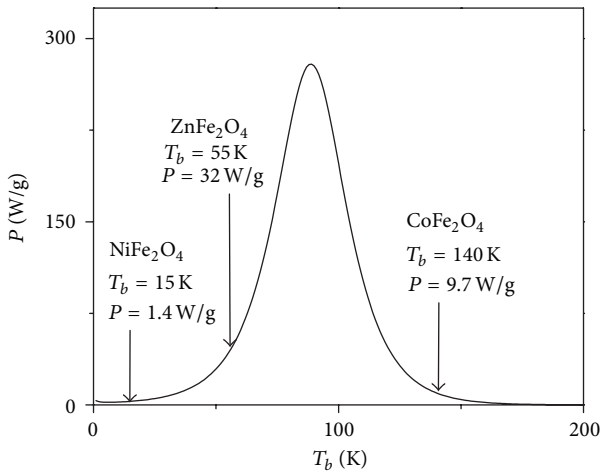

Figure 9: SLP as a function of blocking temperature. The calculations were carried out according to formulae (3)-(4).

in the vicinity of room temperature, and (3) have magnetic susceptibility as large as possible.

4. Conclusions

(1) Weakly agglomerated nanoparticles of AFe_2O_4 (A = Mn, Co, Ni, Zn) spinel ferrites have been synthesized by the method of coprecipitation from nonaqueous solutions with the use of metal nitrites as starting reagents. The particles display quite narrow distribution in size with the average size of a few nanometers. The size and morphology of the synthesized nanoferrites can meet necessary requirements imposed on the nanosized drug deliverers after minor improvement of their uniformity in size.

(2) Characteristic magnetic parameters of the nanoparticles including average magnetic moment of an individual nanoparticle and blocking temperature have been determined from quasistatic magnetic measurements. The specific loss power which is released on the irradiation of an ensemble of particles with an AC magnetic field has been calculated and measured experimentally. The study has shown that Neel absorption mechanism for the superparamagnetic nanoparticles is manifested in Ni, Zn, and Co-containing spinel compounds.

(3) The key parameters responsible for the heating efficiency in AC magnetic field have been determined. The directions to enhance the specific loss power which is released on the irradiation of an ensemble of particles with an AC magnetic field have been outlined.

Conflict of Interests

The authors declare that there is no conflict of interests regarding the publication of this paper.

References

[1] M. M. Rashad and O. A. Fouad, "Synthesis and characterization of nano-sized nickel ferrites from fly ash for catalytic oxidation of CO," *Materials Chemistry and Physics*, vol. 94, no. 2-3, pp. 365–370, 2005.

[2] L. Satyanarayana, K. M. Reddy, and S. V. Manorama, "Nano-sized spinel $NiFe_2O_4$: a novel material for the detection of liquefied petroleum gas in air," *Materials Chemistry and Physics*, vol. 82, no. 1, pp. 21–26, 2003.

[3] S. P. Gubin, Y. A. Koksharov, G. B. Khomutov, and G. Y. Yurkov, "Magnetic nanoparticles: preparation, structure and properties," *Russian Chemical Reviews*, vol. 74, no. 6, pp. 489–520, 2005.

[4] E. H. Frei, E. Gunders, M. Pajewsky, W. J. Alkan, and J. Eshchar, "Ferrites as contrast material for medical X-ray diagnosis," *Journal of Applied Physics*, vol. 39, no. 2, pp. 999–1001, 1968.

[5] M. I. Majeed, Q. Lu, W. Yan et al., "Highly water-soluble magnetic iron oxide (Fe_3O_4) nanoparticles for drug delivery: enhanced in vitro therapeutic efficacy of doxorubicin and MION conjugates," *Journal of Materials Chemistry B*, vol. 1, no. 22, pp. 2874–2884, 2013.

[6] S. Garćia-Jimeno, R. Ortega-Palacios, M. F. J. Cepeda-Rubio, A. Vera, L. Leija, and J. Estelrich, "Improved thermal ablation efficacy using magnetic nanoparticles: a study in tumor phantoms," *Progress in Electromagnetics Research*, vol. 128, pp. 229–248, 2012.

[7] G. T. Landi, "Simple models for the heating curve in magnetic hyperthermia experiments," *Journal of Magnetism and Magnetic Materials*, vol. 326, pp. 14–21, 2013.

[8] X. Zhang, S. Chen, H.-M. Wang et al., "Role of Néel and brownian relaxation mechanisms for water-based Fe_3O_4 nanoparticle ferrofluids in hyperthermia," *Biomedical Engineering—Applications, Basis and Communications*, vol. 22, no. 5, pp. 393–399, 2010.

[9] C. H. Li, P. Hodgins, and G. P. Peterson, "Experimental study of fundamental mechanisms in inductive heating of ferromagnetic nanoparticles suspension (Fe_3O_4 Iron Oxide Ferrofluid)," *Journal of Applied Physics*, vol. 110, no. 5, Article ID 054303, 2011.

[10] O. V. Yelenich, S. O. Solopan, V. V. Trachevskii, and A. G. Belous, "Synthesis and properties of AFe_2O_4 (A = Mn, Fe, Co, Ni, Zn) nanoparticles produced by deposition from diethylene glycol solution," *Russian Journal of Inorganic Chemistry*, vol. 58, no. 8, pp. 901–905, 2013.

[11] O. V. Yelenich, S. O. Solopan, and A. G. Belous, "Polyol synthesis and properties of AFe_2O_4 nanoparticles (A = Mn, Fe, Co, Ni, Zn) with spinel structure," *Solid State Phenomena*, vol. 200, Article ID 149155, pp. 149–155, 2013.

[12] A. Monshi, M. R. Foroughi, and M. R. Monshi, "Modified scherrer equation to estimate more accurately nano-crystallite size using XRD," *World Journal of Nano Science and Engineering*, vol. 2, no. 3, pp. 154–160, 2012.

[13] D. Peddis, F. Orrù, A. Ardu, C. Cannas, A. Musinu, and G. Piccaluga, "Interparticle interactions and magnetic anisotropy in cobalt ferrite nanoparticles: influence of molecular coating," *Chemistry of Materials*, vol. 24, no. 6, pp. 1062–1071, 2012.

[14] S. Solopan, A. Belous, A. Yelenich et al., "Nanohyperthermia of malignant tumors. I. Lanthanum-strontium manganite magnetic fluid as potential inducer of tumor hyperthermia," *Experimental Oncology*, vol. 33, no. 3, pp. 130–135, 2011.

[15] M. Veverka, K. Závěta, O. Kaman et al., "Magnetic heating by silica-coated Co–Zn ferrite particles," *Journal of Physics D: Applied Physics*, vol. 47, no. 6, Article ID 065503, 2014.

[16] S. Chikazumi, *Physics of Ferromagnetism*, edited by C. D. Graham, Oxford University Press, Oxford, UK, 2nd edition, 1997.

[17] A. Pradeep, P. Priyadharsini, and G. Chandrasekaran, "Structural, magnetic and electrical properties of nanocrystalline zinc ferrite," *Journal of Alloys and Compounds*, vol. 509, no. 9, pp. 3917–3923, 2011.

[18] J. P. Singh, G. Dixit, R. C. Srivastava, H. M. Agrawal, V. R. Reddy, and A. Gupta, "Observation of bulk like magnetic ordering below the blocking temperature in nanosized zinc ferrite," *Journal of Magnetism and Magnetic Materials*, vol. 324, no. 16, pp. 2553–2559, 2012.

[19] V. Blanco-Gutierrez, E. Climent-Pascual, M. J. Torralvo-Fernandez, R. Saez-Puche, and M. T. Fernandez-Diaz, "Neutron diffraction study and superparamagnetic behavior of $ZnFe_2O_4$ nanoparticles obtained with different conditions," *Journal of Solid State Chemistry*, vol. 184, no. 7, pp. 1608–1613, 2011.

[20] S. Yoon, "Temperature dependence of magnetic anisotropy constant in cobalt ferrite nanoparticles," *Journal of Magnetism and Magnetic Materials*, vol. 324, no. 17, pp. 2620–2624, 2012.

[21] S. Briceño, W. Brämer-Escamilla, P. Silva et al., "Effects of synthesis variables on the magnetic properties of $CoFe_2O_4$ nanoparticles," *Journal of Magnetism and Magnetic Materials*, vol. 324, no. 18, pp. 2926–2931, 2012.

[22] S. Bedanta and W. Kleemann, "Supermagnetism," *Journal of Physics D: Applied Physics*, vol. 42, no. 1, Article ID 013001, 2009.

[23] W. T. Coffey, Y. P. Kalmykov, and J. T. Waldron, *The Langevin Equation and Methods of Solution*, vol. 4, World Scientific Publishers, Singapore, 2nd edition, 1996, edited by: M. W. Evan.

[24] R. E. Rosensweig, "Heating magnetic fluid with alternating magnetic field," *Journal of Magnetism and Magnetic Materials*, vol. 252, no. 1–3, pp. 370–374, 2002.

[25] J. Carrey, B. Mehdaoui, and M. Respaud, "Simple models for dynamic hysteresis loop calculations of magnetic single-domain nanoparticles: application to magnetic hyperthermia optimization," *Journal of Applied Physics*, vol. 109, no. 8, Article ID 083921, 2011.